Phys Chem Minerals (2018) 45:423–434
DOI 10.1007/s00269-017-0930-1

ORIGINAL PAPER

Single crystal growth, characterization and high-pressure Raman spectroscopy of impurity-free magnesite ($MgCO_3$)

Wen Liang[1] · Zeming Li[1,2] · Yuan Yin[1,2] · Rui Li[1,2] · Lin Chen[1,2] · Yu He[1,3] · Haini Dong[1,3] · Lidong Dai[1] · Heping Li[1]

Received: 9 August 2017 / Accepted: 3 November 2017 / Published online: 11 November 2017

Abstract The understanding of the physical and chemical properties of magnesite ($MgCO_3$) under deep-mantle conditions is highly important to capture the essence of deep-carbon storage in Earth's interior. To develop standard rating scales, the impurity-free magnesite single crystal, paying particular attention to the case of avoiding adverse impacts of Ca^{2+}, Fe^{2+}, and Mn^{2+} impurities in natural magnesite, is undoubtedly necessary for all research of magnesite, including crystalline structural phase transitions, anisotropic elasticity and conductivity, and equation of state (EoS). Thus, a high-quality single crystal of impurity-free magnesite was grown successfully for the first time using the self-flux method under high pressure–temperature conditions. The size of the magnesite single crystal, observed in a plane-polarized microscope, exceeds 200 μm, and the crystal exhibits a rhombohedral structure to cleave along the (101) plane. In addition, its composition of $Mg_{0.999\pm0.001}CO_3$ was quantified through electron probing analysis. The structural property was investigated by means of single crystal X-ray diffraction and the unit cell dimensions obtained in the rhombohedral symmetry of the $R\bar{3}c$ space group are $a=4.6255$ (3) and $c=14.987$ (2), and the final $R=0.0243$ for 718 reflections. High-pressure Raman spectroscopy of the magnesite single crystal was performed up to 27 GPa at ambient temperature. All Raman active bands, ν_i, without any splitting increased almost linearly with increasing pressure. In combination with the high-pressure Raman results $\frac{d\nu_i}{dP}$ and the bulk modulus K_T (103 GPa) reported from magnesite EoS studies, the mode Grüneisen parameters (1.49, 1.40, 0.26, and 0.27) of each vibration (*T*, *L*, ν_4, and ν_1) were calculated.

Keywords Impurity-free magnesite single crystal growth · Single crystal X-ray diffraction · Raman spectroscopy · High pressure

Introduction

Carbonate is one of the most abundant minerals on the earth's surface, and play a key role in the chemistry and dynamics of many geological processes (Oelkers and Cole 2008). Moreover, they may be transferred into the deep-mantle interior by subduction of oceanic lithosphere (Javoy 1997; Brenker et al. 2007; Seto et al. 2008; Litasov and Ohtani 2009). Recently, interest in carbonate minerals in geoscience has grown significantly because the global carbon cycle, in balancing the carbon storage between the earth's surface and deep interior, has been a subject of great concern (Dasgupta and Hirschmann 2010; Hazen et al. 2012). Thus, knowledge of the physical and chemical properties of deep-carbon hosts under deep-mantle conditions is necessary for the understanding of deep-carbon storage and the global carbon cycle (Jana and Walker 1997; Rohrbach and Schmidt 2011). With increasing depth in the earth's interior, especially in the lower mantle, carbon exists in various forms, such as carbonate, carbon-bearing fluid, diamond, and iron carbides (Dasgupta and Hirschmann 2010; Kaminsky and Wirth 2011). Among these carbon-bearing

✉ Heping Li
liheping@vip.gyig.ac.cn

[1] Key Laboratory of High temperature and High pressure Study of the Earth's Interior, Institute of Geochemistry, Chinese Academy of Sciences, Guiyang 550081, China

[2] University of Chinese Academy of Sciences, Beijing 100049, China

[3] Center for High Pressure Science and Technology Advanced Research, Shanghai 201203, China

minerals, magnesite, which remains chemically stable under the high pressure–temperature conditions of the upper and lower mantle, is considered as typical and significant carbon-bearing compound. Thus, it is a possible candidate for stable deep-carbon storage (Katsura and Ito 1990; Isshiki et al. 2004; Litasov et al. 2008; Dasgupta and Hirschmann 2010; Stagno et al. 2011). Meanwhile, there are strong indications that some carbonate inclusions in diamonds from the lower mantle have been observed already; this provides further support that magnesite may be a major host of deep-mantle carbon (McCammon et al. 1997; Pal'yanov et al. 1999; Kaminsky 2012). Hence, studying the properties of magnesite is necessary to elucidate deep-carbon storage in the mantle.

The properties of natural magnesite are well known. However, the impurity-free magnesite single crystal deserves further investigation regarding using it as a standard rating scale by avoiding uncertain influence of Ca^{2+}, Fe^{2+}, and Mn^{2+} impurities in natural magnesite. This facilitates the building of a clear and ideal model for magnesite research. Owing to the unavailability of impurity-free magnesite single crystal, natural magnesite or synthetic polycrystalline magnesite has to be employed to study its physical properties, *P–V–T* EoS, chemical reactions, etc. (Markgraf and Reeder 1985; Zhang et al. 1997, 1998; Isshiki et al. 2004). In this case, some exclusive properties of magnesite single crystal without disturbance from impurities remain unclear. For instance, there has been increasing experimental evidence over recent years that magnesite undergoes crystalline structural phase transitions at high temperatures and very high pressures exceeding 100 GPa (Isshiki et al. 2004; Skorodumova et al. 2005; Oganov et al. 2008). At high pressure–temperature conditions up to 115 GPa and approximately 2100 K, very close to the relevant conditions of the lowermost mantle, magnesite could undergo a structural phase transition to a new structure called magnesite II phase (Isshiki et al. 2004), which was indexed as the basis of the aragonite structure from the observed powder X-ray diffraction peaks. This means that magnesite prefers to stabilize as a smaller-volume phase (aragonite structure) under the lowermost mantle conditions. However, owing to the natural polycrystalline magnesite ($Mg_{0.994}Ca_{0.006}CO_3$) used in this study, a determinate structure of magnesite II phase has not been obtained thus far. As a comparison, to resolve this problem, high pressure–temperature synchrotron X-ray diffraction aimed at the high-quality and impurity-free magnesite single crystal is required. Furthermore, it is not mentioned whether impurity-free magnesite can be stable under higher pressure–temperature conditions because the uncertain influence of 6‰ Ca^{2+} impurities could destroy the structural stability of magnesite. Additional experimental studies demonstrate that the impurity-free magnesite single crystal is necessary for magnesite basic research. In previous studies, EoS studies of magnesite focused entirely on synthetic polycrystalline magnesite (Zhang et al. 1997; Fiquet et al. 2002; Litasov et al. 2008). In particular, EoS of magnesite single crystals without impurities, including more precise, doubtless, and credible structural information, is indispensable to *P–V–T* behavioral assumptions and descriptions of deep-carbon hosts in the earth's interior. Hence, single crystal artificial growth of impurity-free magnesite could provide a basis for magnesite properties, and remains of great importance to continuous studies thereof.

Thus far, the only report of single crystal artificial growth of impurity-free magnesite, as well as single crystal XRD, is stirring by the hydrothermal method (Oh et al. 1973a, b). Although a magnesite single crystal (~ 100 μm) was achieved successfully in this way, there remain some obvious deficiencies. Essentially, the technology and process of single crystal growth is so complex that it could thwart experimental repeatability; thus, single crystal growth of impurity-free magnesite remains a problem that has not been solved effectively. Therefore, it is worth considering the exploration of the new method using the more simple and feasible process for single crystal artificial growth of impurity-free magnesite.

In this paper, we report a simple novel method of magnesite single crystal artificial growth using the self-flux method under high pressure–temperature conditions. The conditions and process of crystal growth are described in detail so as to ensure experimental repeatability. The microcomposition of the single crystal was quantified by electron probing analysis. The result of the infrared spectrum indicates that magnesite single crystals do not contain HCO_3^- or OH^- functional groups. Accurate structural information for magnesite, including lattice parameters, positional and thermal parameters, and bond length and angle, was obtained from single crystal XRD experiments and the corresponding data analysis. High-pressure Raman spectroscopy was performed up to a pressure of 27 GPa and the mode Grüneisen parameter of each vibration was calculated.

Experiment method

The magnesite single crystal was grown by the self-flux method in a sealed environment under high pressure–temperature conditions. The starting material $MgCO_3{\cdot}3H_2O$ (99.9%) was ground in an agate mortar with acetone. A sample pellet was made and sealed into a platinum tube 6 mm in diameter and 3 mm in length. Using h-BN as the pressure medium, the high-pressure experiment was performed on a DS 6 × 600t cubic-anvil-type apparatus with 23.5-mm truncation edge length of WC anvils (maximum possible pressure of 4 GPa), and its pressure was calibrated by Bi-phase transition and chloride (LiCl, KCl, and NaCl) melting curves

at high pressure. A graphite heater (inner and outer diameter of 10 and 12 mm, respectively) and a K-type thermocouple were used in these experiments.

A high-pressure trial synthesis from $MgCO_3 \cdot 3H_2O$ at 4 GPa at various temperatures was conducted to determine the hydrolysis and decomposition temperature. Subsequently, the principle of magnesite single crystal growth in the *P–T* phase diagram is explained to ensure the most appropriate condition for $MgCO_3$ single crystal growth. In this case, the high-pressure experiment was performed at 4 GPa and 1100 °C for 2 h. Afterwards, the crystals were cooled slowly to 800 °C at a cooling rate of 1 °C min^{-1}; then, it was quenched to room temperature and the pressure was released. Finally, the platinum tube was opened and the single crystals were examined and selected under a microscope.

From observation under the plane-polarized microscope, the average size of single crystals reaches 200 μm, with the maximum size exceeding 500 μm. The single crystal exhibits light, colorless and a rhombohedral habit with perfect (101) cleavage. The micro-composition of the single crystal was quantified by electron probing analysis, and the sample composition is $Mg_{0.999\pm0.001}CO_3$.

To quantify the water content of the magnesite single crystal, the infrared spectrum experiment was carried out. Some single crystals were selected and washed in NH_4Cl aqueous solution to clean $Mg(OH)_2$ coverage. Then, the crystals were washed in H_2O for three times and finally dried in an oven at 60 °C for 24 h. A piece of the single crystal (a diameter of ~ 100 μm and a thickness of ~ 40 μm) was cut and prepared for the infrared spectrum. Using $NaHCO_3$ and $Mg(OH)_2$ as the references of hydroxyl (OH^-), the infrared spectrum experiment was performed on a Fourier transform infrared spectrometer (VERTEX 70, BRUKER).

Single crystal XRD measurements were conducted at ambient pressure using a four-circle BRUKER diffractometer equipped with a SMART APEX-CDD detector using MoKα radiation in China University of Geosciences, Beijing. A piece of the single crystal (~ 100 μm) was cut and prepared for the single crystal XRD experiment. A total of 718 reflections were collected during the whole process, and the reflection intensities were measured by scanning the narrow frames. The structures were solved by the direct method and refined by full matrix least squares using SHELXTL5.1 software. Meanwhile, the anisotropic thermal parameters were refined using the *x*-coordinate of oxygen.

For Raman spectroscopic experiments, a piece of the single crystal with a diameter of ~ 80 μm and a thickness of ~ 30 μm was cleaved along the (101) rhombohedral plane and used as the starting sample. A rhenium gasket was pre-indented to a thickness of 60 μm by a pair of diamond anvils with 400 μm flat culets. A hole of 150 μm in diameter was drilled in the pre-indented gasket and used as a sample chamber. The starting sample was loaded into the sample chamber of a DAC with the (101) crystal plane facing the culet, together with two ruby spheres close to the sample as the pressure calibrant. Neon was loaded into the sample chamber as the pressure medium, using a high-pressure gas loader in the Center for High Pressure Science and Technology Advanced Research, Shanghai.

The Raman system used for the experiments is a Renishaw 2000 micro-confocal laser Raman spectrometer equipped with a charge-coupled device detector, a 2400 lines mm^{-1} diffraction grating and a holographic notch filter. The spectrum physics model of a 2017 argon ion laser operating at 514.5 nm was used as the excitation source. The laser power was limited to 30 mW to avoid overheating of the sample and the zero-offset was calibrated using a silicon single crystal at 520.0 cm^{-1}. Scattered radiation was collected by an Olympus microscope 20× at an ultra-length working distance objective through backscattering. Each Raman spectrum was collected at an exposure time of 10 min to ensure quality data analyses. The pressure and error, thereof, was quantified from the average pressure value given by the ruby sphere of Raman pre-test and post-test.

Results and discussion

Impurity-free $MgCO_3$ single crystal growth by the self-flux method

In this particular case of $MgCO_3$, single crystal growth using the traditional flux method is expected to be quite difficult owing to difficulty in controlling the experimental conditions to cause melting of $MgCO_3$. According to the results of the TG analysis (Liang et al. 2017), the thermal stability of $MgCO_3$ is relatively poor and its decomposition temperature is rather low (~ 400 °C). In this case, its theoretical melting point is considerably higher than its decomposition temperature to the extent that reaching its melting point directly while maintaining its stability is unattainable. In conclusion, it is incredibly difficult, or almost impossible, to grow $MgCO_3$ single crystals through $MgCO_3$ melts under ambient conditions.

Therefore, the determination of an available flux to reduce the $MgCO_3$ melting point is the key to $MgCO_3$ single crystal growth by the flux method. Significantly, based on previous studies, the existence of $Mg(OH)_2$ or liquid water can greatly reduce the melting point of calcite and dolomite (Irving and Wyllie 1975; Dalton and Wood 1993). We suspect that, as a comparative available flux, hydroxyl (OH^-) or constitutional water could also reduce the melting point of $MgCO_3$ effectively. With regards to an ideal starting material for $MgCO_3$ single crystal growth, magnesium carbonate tri-hydrates ($MgCO_3 \cdot 3H_2O$) can be used because it not only provides the required chemical composition of $MgCO_3$, but also, in

particular, has the effect of an available (self-) flux attributed to the constitutional water contained. Accordingly, the self-flux method is more favorable for growing single crystals because no additional flux material, such as $Mg(OH)_2$, is used so as to avoid separation of $MgCO_3$ and residual flux material. Compared with the traditional solid flux method at high pressure, the fluid flux (constitutional water) could greatly reduce the residual stress in single crystals to ensure the highest quality crystals possible.

Moreover, the additional attention is highly deserved to suppress the hydrolysis reaction in $MgCO_3{\cdot}3H_2O$ substantially because $MgCO_3$-series materials are so sensitive to hydrolysis reaction that they always form magnesium carbonate hydrates or basic magnesium carbonate; this occurs despite the fact that numerous magnesite crystals have a stable nature and their chemical stability exhibits almost no significant difference in attribution from other carbonates, such as $CaCO_3$, $SrCO_3$, and $BaCO_3$. In accordance with previous studies, the hydrolysis reaction in $MgCO_3{\cdot}3H_2O$ can be effectively and completely suppressed under the high pressure–temperature conditions owing to the high-pressure stability of $MgCO_3$ (Liang et al. 2017).

Using a high-pressure dehydration reaction, a series of samples were synthesized from $MgCO_3{\cdot}3H_2O$ at 4 GPa at various reaction temperature to quantify the $MgCO_3$ decomposition temperature and $MgCO_3{\cdot}3H_2O$ hydrolysis temperature; the powder XRD results are shown in Fig. 1a. At 4 GPa and 800–1100 °C for 1 h, the as-synthesized samples were identified as $MgCO_3$ without any impurity. By controlling the reaction temperature, the impurity identified as $Mg(OH)_2$ caused by the hydrolysis reaction was observed at 700 °C, whereas $MgCO_3$ was decomposed into MgO at 1200 °C. Combined with the results at 1–3 GPa (Liang et al. 2017), an approximate $MgCO_3 + H_2O$ phase stability in the *P–T* phase diagram was obtained, as shown in Fig. 1b, in which the decomposition and hydrolysis curves are represented by the red and blue dash lines, respectively. It is known from the *P–T* phase diagram that the region of $MgCO_3$ phase stability lies between the blue and red dash lines. The melting curve is represented by the black dash line, which is reduced below the decomposition temperature on the diagram owing to the use of constitutional water flux. As a result, $MgCO_3$ can be melted on the premise of its chemical stability; thus, it is reasonable that the most appropriate condition at 4 GPa for $MgCO_3$ single crystal growth is the range of 800–1100 °C in the presence of constitutional water flux.

Composition and morphology of the magnesite single crystal

By controlling the pressure, temperature, and cooling rate, magnesite single crystals were achieved successfully using the self-flux method. A whole single crystal (~ 500 μm) without any disposal was prepared for a thin section. Unfortunately, it smashed into several pieces (~ 100 μm), as shown in Fig. 2a, because $MgCO_3$ material is highly brittle and easily crushed during polishing. Nevertheless, the micro-composition of single crystals was quantified by electron probing analysis. Figure 2b shows the backscattering electronic (BSE) image and the detection position on the $MgCO_3$ single crystal thin section, whereas the results of the analysis of the Mg content is given in Table 1. It is

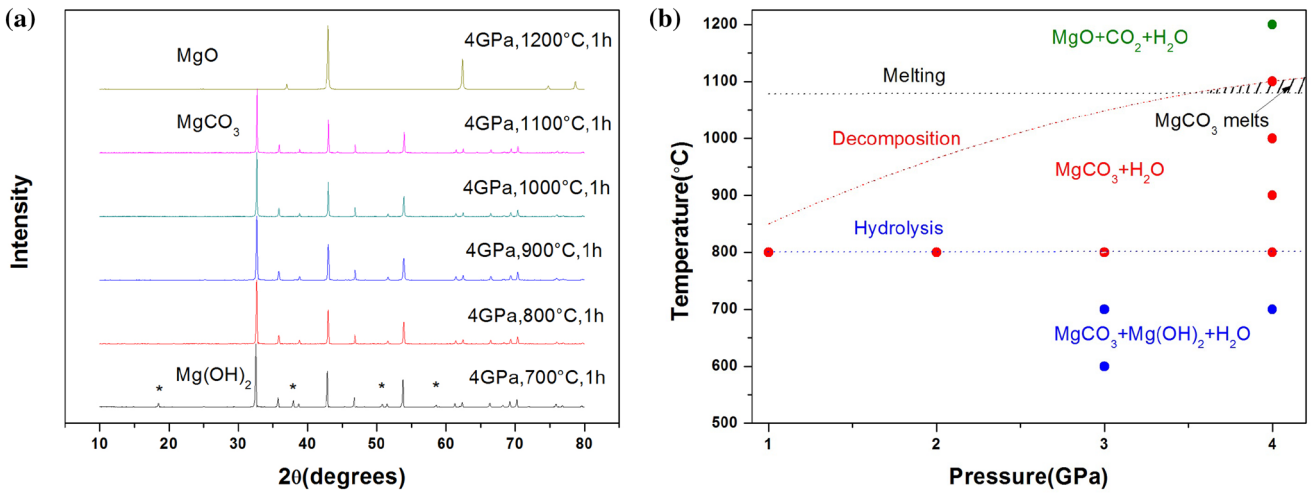

Fig. 1 **a** Powder X-ray diffraction for a series of samples synthesized under the various temperature at 4 GPa for 1 h. The impurity marked by asterisk (*) is identified as $Mg(OH)_2$. **b** The *P–T* phase diagram of $MgCO_3 + H_2O$, in which the decomposition curve is given by the red dash line and the blue dash line is the hydrolysis curve, respectively. Diagrammatically, the melting curve is marked by the black dash line, which is reduced below the decomposition line due to water flux using, and the shadow refers to the possible region of $MgCO_3$ melts. The results at 1–3 GPa were given by Liang et al. (2017)

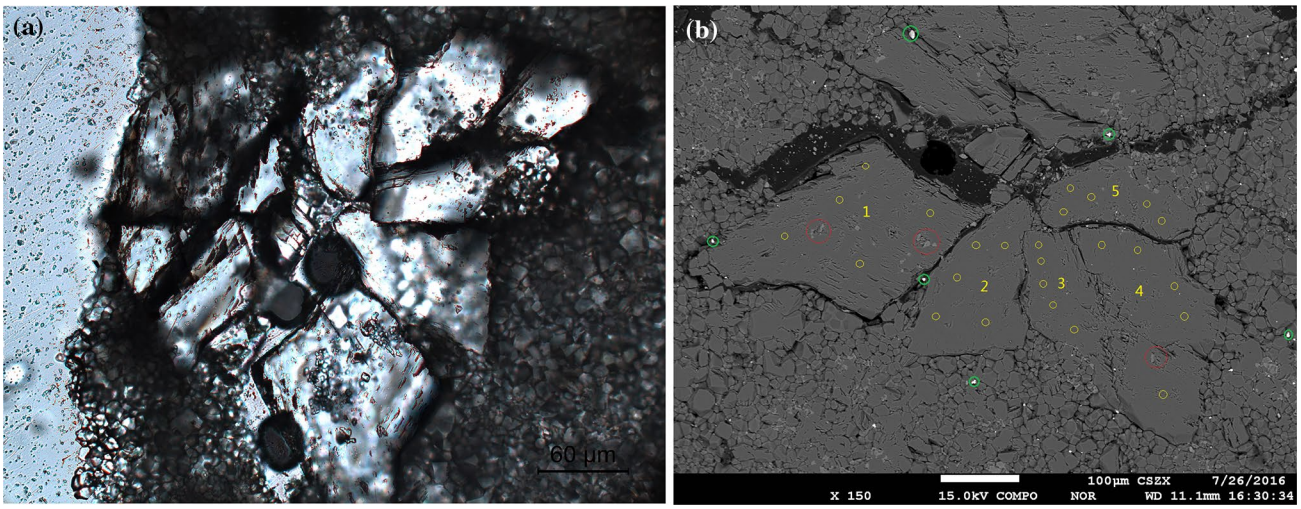

Fig. 2 **a** The micrograph for magnesite single crystal thin section under plane-polarized microscope. **b** The backscattered electronic (BSE) image of magnesite single crystal thin section, in which the yellow circles are the detection position of electron probing. The white parts, marked by green circles, were identified as Cr_2O_3 coming from the remnants of grinding papers, and the water-eroded-like parts, marked by red circles, were identified as $Mg(OH)_2$ caused by the slight hydrolysis reaction

Table 1 Results of electron probe analysis of magnesite single crystal thin section

MgO Mass %	Position 1	Position 2	Position 3	Position 4	Position 5	Average	Composition
Region 1	47.79	47.67	47.83	47.85	47.74	47.78 ± 0.07	$Mg_{0.9993\pm0.0016}CO_3$
Region 2	47.81	47.75	47.63	47.77	47.80	47.75 ± 0.06	$Mg_{0.9989\pm0.0012}CO_3$
Region 3	47.74	47.73	47.82	47.77	47.79	47.77 ± 0.05	$Mg_{0.9992\pm0.0011}CO_3$
Region 4	47.69	47.75	47.75	47.67	47.78	47.73 ± 0.05	$Mg_{0.9983\pm0.0012}CO_3$
Region 5	47.75	47.82	47.65	47.76	47.78	47.75 ± 0.07	$Mg_{0.9989\pm0.0014}CO_3$
Average	–	–	–	–	–	47.76 ± 0.06	$Mg_{0.9990\pm0.0013}CO_3$

observed from BSE image using MgO as the standard sample that the gray scales of the polished surfaces of single crystal pieces exhibit almost no difference; this implies that the single crystals have the same Mg content. It is worth noting that the abnormal and white parts marked by green circles were identified as Cr_2O_3, derived from the remnants of grinding papers. A few water-eroded-like parts, marked by red circles, were identified as $Mg(OH)_2$ attributed to the slight hydrolysis reaction caused by the high pressure–temperature gradient from the Φ6 × 3 mm large sample volume, which was designed to ensure the largest $MgCO_3$ single crystal possible. The existence of a little $Mg(OH)_2$ does not affect the properties of $MgCO_3$ single crystals because $MgCO_3$ and $Mg(OH)_2$ were separated and did not form as a solid solution. Actually, the smaller single crystals, which do not contain $Mg(OH)_2$ such as the nos. 2 or 4 regions, were selected or cut from a larger crystal, or even a little $Mg(OH)_2$ coverage was washed off completely by NH_4Cl aqueous solution. A total of 25 points in five different areas, marked by yellow circles, were selected for electron probing analysis. Finally, the average mass fraction of MgO obtained is 47.76 ± 0.06% and the single crystal composition was calculated as $Mg_{0.999\pm0.001}CO_3$, which is in agreement with the stoichiometric in the error range.

Figure 3 shows the micrograph from the plane-polarized microscope with (a) reflected light and (b) transmitted light. A piece of single crystal (~ 200 μm) was seen as a bright and colorful halo in the reflected light, while it was observed clearly in the transmitted light that it exhibits a rhombohedral structure with a 120° edge angle and is cleaved along the (101) plane, which is considered to be cleaving behavior of the natural calcite-type minerals.

Infrared spectrum of the magnesite single crystal

In the range of 3000–4000 cm^{-1}, shown in Fig. 4, the characteristic peaks of OH^- are observed from the infrared spectrum of $NaHCO_3$ and $Mg(OH)_2$, and in comparison, no remarkable peak is observed from the infrared spectrum of magnesite crystal, which indicates that magnesite crystals,

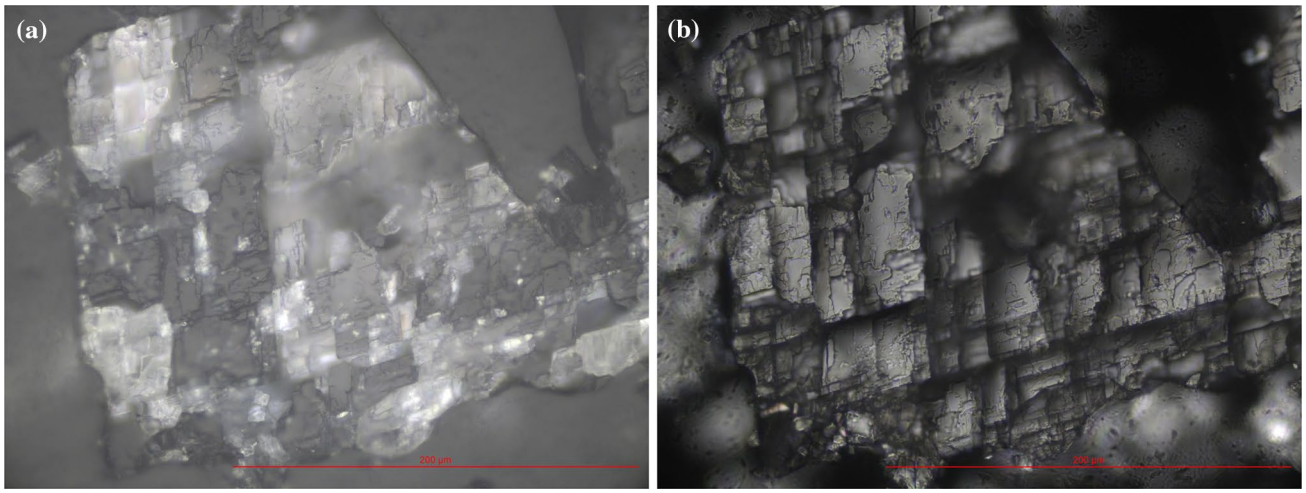

Fig. 3 The micrograph for a piece of magnesite single crystal (~200 μm) under plane-polarized microscope with reflected light (**a**) and transmitted light (**b**). Obviously, the single crystal exhibits the rhombohedral structure with 120° edge angle and cleaved along the (101) plane

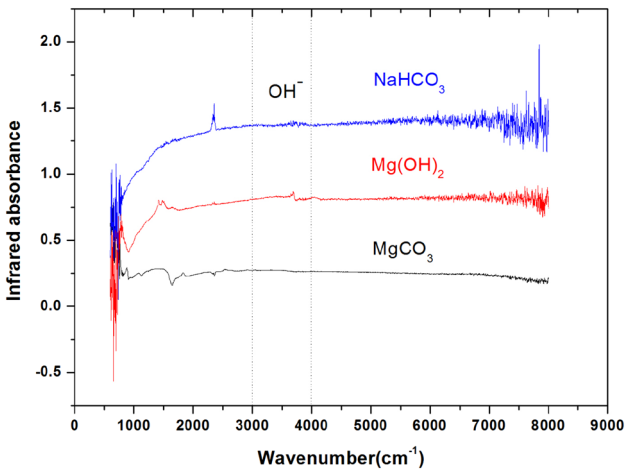

Fig. 4 The infrared spectrum of magnesite single crystal, together with the results of $NaHCO_3$ and $Mg(OH)_2$ as the references of OH^-

we obtained, do not contain HCO_3^- or OH^- functional groups and can be considered as an anhydrous mineral.

$MgCO_3$ single crystal XRD and structural characterization

Although the single crystal structure of impurity-free $MgCO_3$ was determined by Oh et al. (1973a, b), there remain some obvious deficiencies resulting from the limitations in experimental conditions or equipment at that time. For example, the cell dimensions with $a = 4.637$ (l) and $c = 15.023$ (3) were obtained using the powder method and the symmetry of the $R\bar{3}c$ space group was confirmed with a photographic experiment, but certainly not analyzed, in this particular case, by the direct method from single crystal XRD data. For comparison, the intensities of many sufficient reflections without any splitting or trailing field, shown in Fig. 5a, were collected from single crystal XRD in our work to ensure accurate and reasonable results. Crystal data and structure refinement, including lattice parameters, positional and thermal parameters, and bond length and angle, are summarized in Table 2, together with the results by OH Ki Dong. Figure 5b shows the rhombohedral structure of the magnesite crystal, as well as the coordination relations. The rhombohedral magnesite unit cell consists of CO_3^{2-} anions and Mg^{2+} cations; obviously, the central Mg^{2+} cation is six-coordinated with (MgO_6) octahedron geometry, as well as the bond angle of O–Mg–O. Significantly, the accurate structural data of magnesite crystal provides a standard rating scale in mineralogy and it could form a basis for magnesite research.

High-pressure Raman spectroscopy and the mode Grüneisen parameters

The Raman spectra of the magnesite single crystal has been measured at ambient pressure, and its spectra are already well known as a calcite-type minerals (Rutt and Nicola 1974; Edwards et al. 2005; Gunasekaran et al. 2006; Rividi et al. 2010; Kaabar et al. 2011). Six Raman active vibrations (T, L, ν_4, ν_1, ν_3, $2\nu_2$) in the wavelength range of 100–2000 cm^{-1}, shown in Fig. 6a, are dominated by the peaks located at 212, 330, 738, 1093, 1445, and 1762 cm^{-1}, which were fitted with a Lorentzian function. The peaks at 212 and 330 cm^{-1} are derived mainly from translational lattice mode T and librational lattice mode L, respectively. The peaks at 738 cm^{-1} comes from in-plane bending internal mode ν_4. The peaks with the strongest feature located at 1093 cm^{-1} are caused by symmetric stretching of internal mode ν_1. Similarly, the

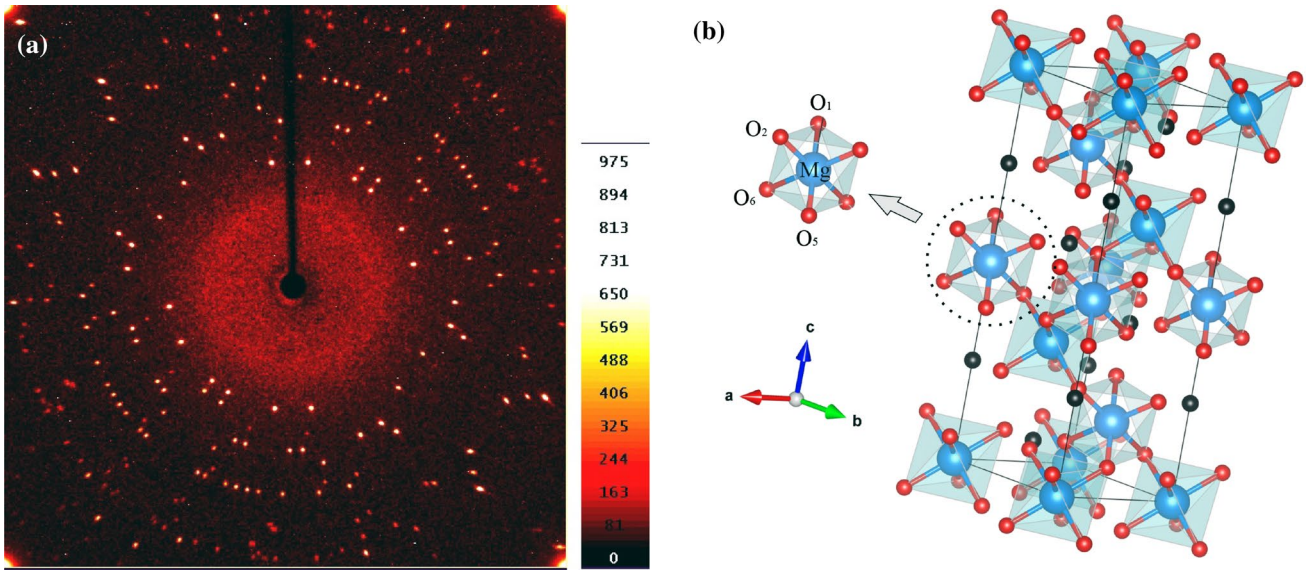

Fig. 5 **a** The intensities of many enough reflections without any splitting or trailing field collected from single crystal XRD. **b** The rhombohedral structure of magnesite crystal as well as the coordination relations between Mg^{2+} and CO_3^{2-}

peaks at 1445 and 1762 cm^{-1} are attributable to the anti-symmetric stretching mode ν_3 and out-of-plane bend $2\nu_2$, respectively.

The calcite-type carbonate minerals ACO_3 (A–Ca, Mg, Fe, Mn) have the common rhombohedral structure (Fig. 5b) and the feature of this structure is that the separate carbonate ion groups CO_3^{2-} are bound to the crystal lattice by strong internal C–O bonds and weaker cation–oxygen bonds. From the previous studies, six Raman active vibrations (*T*, *L*, ν_4, ν_1, ν_3, $2\nu_2$) are closely related to carbonate ion (Bischoff et al. 1985; Schauble et al. 2006). Due to very high geometric symmetry with 120° bond angle of carbonate ion, C–O bond length seems to be an effective function to impact Raman frequency, whereas C–O bond length can be controlled by cation size. To take symmetric stretching mode ν_1 as an example, calcite has much larger cation size than magnesite, but in the opposite sense it has lower Raman frequency (1085 cm^{-1} for calcite and 1093 cm^{-1} for magensite), and thus much larger C–O bond length is corresponding to lower Raman frequency (Goldsmith and Heard 1961; Zolotoyabko et al. 2010; Floquet et al. 2015; Perrin et al. 2016). Similarly, the pressure also can be a factor changing C–O bond and the effect of the pressure on compressibility of C–O bonds length makes Raman vibrations shift to higher frequency (Boulard et al. 2012). Subsequently, high-pressure Raman spectra of the magnesite single crystal were measured up to 27 GPa with 1–2 GPa pressure steps at room temperature. Four Raman active bands, which were identified as translational lattice mode *T*, librational lattice mode *L*, in-plane bending internal mode ν_4, and symmetric stretching internal mode ν_1, were observed. Two other Raman active modes, the anti-symmetric stretch ν_3 and out-of-plane bend $2\nu_2$, were not observed in this study owing to limitations in the diamond windows. In the pressure range over which the spectra of magnesite were measured, all observed Raman bands increased continuously and almost linearly with increasing pressure and did not undergo any resolvable splitting, as would be a concern just as a phase transition occurred in ferromagnesite at high pressure (Lavina et al. 2009; Lin et al. 2012). The linear relationship between each measured vibrational frequency ν_i and the pressure *P*, given in Fig. 6b, c and Table 3, can be fitted. The value of slope $d\nu_i/dP$ obtained is slightly difference from the results of the nature magnesite reported previously (Williams et al. 1992; Gillet et al. 1993), which could be caused by the effect of impurities and the difference of pressure medium. In the future, the relationship between C–O bond length and pressure will be systematically studied in EoS of magnesite single crystals, and furthermore, the relationship between C–O bond length and Raman vibrations can also be determined precisely, which can be useful for explaining the micro-mechanism of Raman vibrations in carbonate minerals.

As a very important thermodynamic parameters for describing the high pressure–temperature behavior of minerals, the mode Grüneisen parameter provides a means by which the relative contributions of each vibration to the thermochemical properties are established (Anderson 2000). The parameter links the variation of frequency ν_i to the variation in crystal lattice volume $V(P, T)$ and even the effect of changing temperature on the size or dynamics of the lattice; thus, it is a function of pressure *P* for the isothermal state or volume *V* for isobaric state (Wagner

Table 2 Crystal data and structure refinement of magnesite single crystal, including space group, lattice parameters, positional and thermal parameters, bond length and bond angle, together with the results by Oh et al. (1973a, b)

Composition $MgCO_3$							
Space group $R\bar{3}c$ (no. 167)							
Lattice parameters							
a	*b*	*c*	*α*	*β*	*γ*	*R*	
4.6255 (3)	4.6255 (3)	14.987 (2)	90	90	120	0.0243	This work
4.637 (1)	4.637 (1)	15.023 (3)	90	90	120	0.037	OH Ki Dong et al. (1973)

Positional and thermal parameters [This work ($R=0.0243$)]			
Parameters	Mg	C	O
x	0	0	0.27772 (15)
y	0	0	0
z	0	0.25	0.25
U11	0.0058 (3)	0.0059 (5)	0.0054 (3)
U22	0.0058 (3)	0.0059 (5)	0.0079 (3)
U33	0.0067 (4)	0.0047 (7)	0.0090 (4)
U23	0.0000	0.0000	− 0.00115 (18)
U13	0.0000	0.0000	− 0.0058 (9)
U12	0.00289 (14)	0.0030 (2)	0.00393 (17)
Oh et al. (1973a, b) ($R=0.037$)			
x	0	0	0.2767 (2)
y	0	0	0
z	0	0.25	0.25
U11	0.0063 (4)	0.0072 (8)	0.0059 (3)
U22	–	–	0.0091 (4)
U33	0.0060 (3)	0.0052 (6)	0.0083 (3)
U23	–	–	− 0.0027 (9)

	This work	Oh et al. (1973a, b)
Bond distance (Å) and angle (°)		
Mg–O	2.0976 (4)	2.105 (1)
C–O	1.2846 (7)	1.283 (1)
O1–M–-O2	88.180 (11)	88.25 (2)
O1–Mg–O6	91.820 (11)	91.75 (2)
O1–Mg–O5	180.000 (13)	180.00 (2)

2000). As a result, the parameter not only presents the differing mass and ionic radius of substituting cations in magnesite, but also reflects the compressing effect of the carbonate ion. For isothermal expression at constant *T*, the measured vibrational frequency ν_i as a function of pressure *P* represents a mode Grüneisen parameter for the phonon mode, as in the following equation (Born and Huang 1954)

$$\gamma_i = \frac{K_T}{\nu_{i,0}} \cdot \frac{d\nu_i}{dP},$$

where γ_i is the mode Grüneisen parameter, K_T is the isothermal bulk modulus, $\nu_{i,0}$ is each vibration frequency at ambient pressure, and $d\nu_i/dP$ is the slope of each vibration shift with pressure.

The combined high-pressure Raman results ($\frac{d\nu_i}{dP}$) and the reported bulk modulus $K_T = 103$ (1) GPa from the EoS studies of magnesite (Zhang et al. 1997; Isshiki et al. 2004) are used to derive the mode Grüneisen parameter (γ_i), given in Table 4. The mode Grüneisen parameters for the two external lattice modes (*T* and *L*) are 1.49 and 1.40, and accordingly, for the two internal modes (ν_1 and ν_4) are 0.27 and 0.26, respectively. Conclusively, the lower frequency lattice modes (*T* and *L*) of magnesite have mode Grüneisen

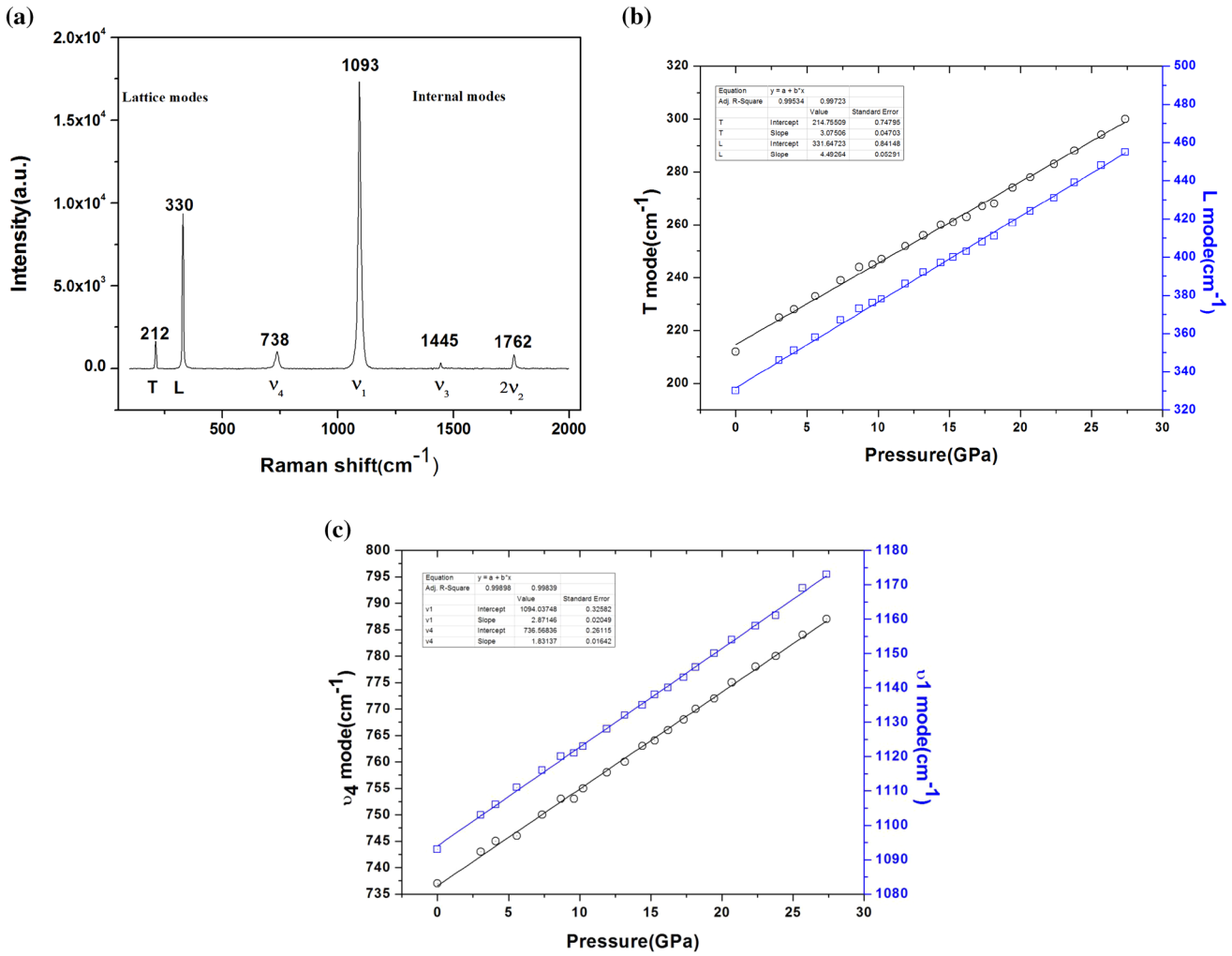

Fig. 6 **a** Raman spectra of magnesite single crystal at ambient conditions. **b** The linear relationship between the measured lattice modes (T and L) and the pressure P. The error bars of the pressure P are smaller than the pressure P and not given. **c** The linear correlation between the measured internal modes (ν_1 and ν_4) and the pressure P. The error bars of the pressure P are smaller than the pressure P and not given

parameters of approximately five times greater than those of the higher frequency internal modes (ν_1 and ν_4).

Mineralogical and geochemical implications

A standard rating scale for magnesite research in mineralogy

Magnesite is a possible candidate for the stable carbon host at lower mantles. Thus, the anisotropic elasticity and conductivity, as well as thermal and structural properties of magnesite, remain worthy of deep investigation. In spite of the large amount of experimental data and reports acquired over the last decades, synthetic polycrystalline magnesite or natural magnesite had to be employed. The major reason is that the single crystal of impurity-free magnesite is unavailable and the single crystal growth is always difficult in materials science. Therefore, it is too difficult to establish and ensure a unified standard in magnesite research. Thus, for a standard rating scale in mineralogy, essentially, impurity-free magnesite single crystals provide ideal models by avoiding the influence of impurities, and form the basis of more reliable experimental data, especially for the studies of the anisotropic elasticity C_{ij} and conductivity σ_{ij}.

Table 3 The data of high-pressure Raman spectra, including the value of four observed Raman bands (*T*, *L*, ν_4, ν_1) with the corresponding pressure and the error bars of the pressure

Pressure (GPa)	T (cm^{-1})	L (cm^{-1})	ν_4 (cm^{-1})	ν_1 (cm^{-1})
1 atm	212	330	738	1093
3.05 (±0.03)	225	346	743	1103
4.08 (±0.05)	228	351	745	1106
5.58 (±0.06)	233	358	746	1111
7.36 (±0.04)	239	367	750	1116
8.68 (±0.03)	244	373	753	1120
9.60 (±0.05)	245	376	753	1121
10.24 (±0.02)	247	378	755	1123
11.91 (±0.03)	252	386	758	1128
13.17 (±0.04)	256	392	760	1132
14.41 (±0.05)	260	397	763	1135
15.27 (±0.04)	261	400	764	1138
16.21 (±0.02)	263	403	766	1140
17.31 (±0.05)	267	408	768	1143
18.15 (±0.03)	268	411	770	1146
19.45 (±0.02)	274	418	772	1150
20.69 (±0.07)	278	424	775	1154
22.37 (±0.05)	283	431	778	1158
23.79 (±0.07)	288	439	780	1161
25.68 (±0.08)	294	448	784	1169
27.35 (±0.08)	300	455	787	1173

Possible existence of carbonate melts under high-pressure–temperature in the presence of fluid water

The single crystal of magnesite was grown successfully using water fluid flux to melt $MgCO_3$ under high pressure–temperature conditions. In this regard, a possible explanation for the self-existent carbonate melts in nature is that, at convergent plate boundaries, many sedimentary carbonates in subducted oceanic slabs may survive in the forearc or subarc regions of subduction zones, and then be subducted into the deeper mantle. In the particularly hot subduction zone, thermal relaxation could liberate these sedimentary carbonates in the form of carbonate melts through metamorphic dehydration reactions in the subducting oceanic crust and mantle (Poli and Schmidt 2002; Hacker et al. 2003). Hence, it provides a possibility or evidence that the carbonate melts could be formed under high pressure–temperature conditions in the presence of water fluid, and this result is highly consistent with the experimental conditions of $MgCO_3$ single crystal growth. Suggestively, the method of water fluid flux at high pressure–temperature could be used for reference or evaluation of single crystal growth of some other important carbonates, such as impurity-free siderite ($FeCO_3$) or ferromagnesite ($Mg_{1-x}Fe_xCO_3$).

Conclusion

A novel process has been devised to grow impurity-free magnesite single crystals successfully, using the self-flux method under high pressure–temperature conditions. Moreover, it could provide a standard rating scale in mineralogy for magnesite research by avoiding the negative influence of impurities. The excellent and exclusive properties of impurity-free magnesite single crystals, including anisotropic measurement, single crystal EoS studies, and magnesite II structural phase transition, should be investigated further.

Table 4 The calculation of Mode Grüneisen parameter (γ_i) for each Raman band (*T*, *L*, ν_4, ν_1), here select the bulk modulus K_T value of 103 (1) GPa from the studies of magnesite EoS (Zhang et al. 1997), together with the results of $\frac{d\nu_i}{dP}$ from previous studies (Williams et al. 1992; Gillet et al. 1993) for comparison

Raman mode	$\nu_{i,0}$ (cm^{-1})	$\frac{d\nu_i}{dP}$ (cm^{-1}/GPa)	Mode Grüneisen parameter (γ_i)
T	212	3.08 (±0.05)	1.49 ± 0.02
L	330	4.49 (±0.05)	1.40 ± 0.02
ν_4	738	1.83 (±0.02)	0.26 ± 0.01
ν_1	1093	2.87 (±0.02)	0.27 ± 0.01
	$\frac{d\nu_i}{dP}$ (cm^{-1}/GPa) in this study	$\frac{d\nu_i}{dP}$ (cm^{-1}/GPa) by Williams et al. (1992)	$\frac{d\nu_i}{dP}$ (cm^{-1}/GPa) by Gillet et al. (1993)
Pressure medium	Ne	Methanol-ethanol	KBr
T	3.08 (±0.05)	2.6 (±0.2)	4.4 (±0.4)
L	4.49 (±0.05)	4.7 (±0.1)	4.5 (±0.3)
ν_4	1.83 (±0.02)	1.5 (±0.2)	1.4 (±0.2)
ν_1	2.87 (±0.02)	2.3 (±0.1)	2.5 (±0.3)

Acknowledgements We thank Dongzhou Zhang and another reviewer for their very helpful comments. We acknowledge Jun-fu Lin from University of Texas at Austin for constructive discussion in carbonate minerals, Zengsheng Li from the Testing Center of Shandong Bureau of China Metallurgy and Geology for composition analysis by electron probe, and Guowu Li and Lin Li from China University of Geosciences for experimental assistance in single crystal XRD. We thank Yong Meng and Jiali Cai from Institute of Geochemistry, Chinese Academy of Sciences, Guiyang, for his valued assistance. This work was financially supported by 135 Program of the Institute of Geochemistry (Y2ZZ041000), CAS, the Strategic Priority Research Program (B) of Chinese Academy of Sciences (XDB18000000), the National Key Research and Development Plan (2016YFC0600100), and Large-scale Scientific Apparatus Development Program (YZ200720), CAS.

References

Anderson OL (2000) The Grüneisen ratio for the last 30 years. Geophys J Int 143:279–294

Bischoff WD, Sharma SK, Mackenzie FT (1985) Carbonate ion disorder in synthetic and biogenic magnesian calcites—a Raman spectral study. Am Miner 70(5–6):581–589

Born M, Huang K (1954) Dynamical theory of crystal lattices. Oxford University Press, UK

Boulard E, Menguy N, Auzende A, Benzerara K, Bureau H, Antonangeli D, Corgne A, Morard G, Siebert J, Perrillat JP, Guyot F, Fiquet G (2012) Experimental investigation of the stability of Fe-rich carbonates in the lower mantle. J Geophys Res Solid Earth (1978–2012), 117(B2)

Brenker FE, Vollmer C, Vincze L, Vekemans B, Szymanski A, Janssens K, Szaloki I, Nasdala L, Joswig W, Kaminsky F (2007) Carbonates from the lower part of transition zone or even the lower mantle. Earth Planet Sci Lett 260:1–9

Dalton JA, Wood BJ (1993) The compositions of primary carbonate melts and their evolution through Wallrock reaction in the mantle. Earth Planet Sci Lett 119:511–525

Dasgupta R, Hirschmann MM (2010) The deep carbon cycle and melting in Earth's interior. Earth Planet Sci Lett 298:1–13

Edwards HGM, Jorge Villar SE, Jehlicka J, Munshi T (2005) FT-Raman spectroscopic study of calcium-rich and magnesium-rich carbonate minerals. Spectrochim Acta Part A 61:2273–2280

Fiquet G, Guyot F, Kunz M, Matas J, Andrault D, Hanfland M (2002) Structural refinements of magnesite at very high pressure. Am Miner 87:1261–1265

Floquet N, Vielzeuf D, Ferry D, Ricolleau A, Heresanu V, Perrin J, Laporte D, Fitch AN (2015) Thermally induced modifications and phase transformations of red coral Mg-calcite skeletons from infrared spectroscopy and high resolution synchrotron powder diffraction analyses. Cryst Growth Des 15(8):3690–3706

Gillet P, Biellmann C, Reynard B, McMillan P (1993) Raman spectroscopic studies of carbonates Part I: high-pressure and high-temperature behaviour of calcite, magnesite, dolomite and aragonite. Phys Chem Miner 20:1–18

Goldsmith JR, Heard HC (1961) Subsolidus phase relations in the system. J Geol 69:45–74

Gunasekaran S, Anbalagan G, Pandi S (2006) Raman and infrared spectra of carbonates of calcite structure. J Raman Spectrosc 37:892–899

Hacker BR, Peacock SM, Abers GA, Holloway SD (2003) Subduction factory 2. Are intermediate-depth earthquakes in subducting slabs linked to metamorphic dehydration reactions? J Geophys Res 108:B1

Hazen RM, Hemley RJ, Mangum AJ (2012) Carbon in Earth's interior: storage, cycling, and life. Eos Trans Am Geophys Union 93(2):17–18

Irving AJ, Wyllie PJ (1975) Subsolidus and melting relationships for calcite, magnesite and the join $CaCO_3$–$MgCO_3$ to 36 kb. Geochim Cosmochim Acta 39:35–53

Isshiki M, Irifune T, Hirose K, Ono S, Ohishi Y, Watanuki T, Nishibori E, Takata M, Sakata M (2004) Stability of magnesite and its high-pressure form in the lowermost mantle. Nature 427:60–63

Jana D, Walker D (1997) The impact of carbon on element distribution during core formation. Geochim Cosmochim Acta 61(13):2759–2763

Javoy M (1997) The major volatile elements of the earth: their origin, behaviour, and fate. Geophys Res Lett 24:177–180

Kaabar W, Botta S, Devonshire R (2011) Raman spectroscopic study of mixed carbonate materials. Spectrochim Acta Part A 78:136–141

Kaminsky F (2012) Mineralogy of the lower mantle: a review of 'super-deep' mineral inclusions in diamond. Earth Sci Rev 110(1–4):127–147

Kaminsky FV, Wirth R (2011) Iron carbide inclusions in lower-mantle diamond from Juina, Brazil. Can Mineral 49:555–572

Katsura T, Ito E (1990) Melting and subsolidus phase-relations in the MgSiO3-$MgCO_3$ system at high-pressures: Implications to evolution of the Earth's atmosphere. Earth Planet Sci Lett 99:110–117

Lavina B, Dera P, Downs RT, Prakapenka V, Rivers M, Sutton S, Nicol M (2009) Siderite at lower mantle conditions and the effects of the pressure-induced spin-pairing transition. Geophys Res Lett 36:L23306

Liang W, Yin Y, Wang L, Chen L, Li H (2017) A new method of preparing anhydrous magnesium carbonate ($MgCO_3$) under high pressure and its thermal property. J Alloys Compd 702:346–351

Lin J-F, Liu J, Jacobs C, Prakapenka VB (2012) Vibrational and elastic properties of ferromagnesite across the electronic spin-pairing transition of iron. Am Mineral 97:583–591

Litasov KD, Ohtani E (2009) Solidus and phase relations of carbonated peridotite in the system CaO–Al_2O_3–MgO–SiO_2–Na_2O–CO_2 to the lower mantle depths. Phys Earth Planet Inter 177:46–58

Litasov KD, Fe Y, Ohtani E, Kuribayashi T, Funakoshi K (2008) Thermal equation of state of magnesite to 32 GPa and 2073 K. Phys Earth Planet Inter 168:191–203

Markgraf SA, Reeder RJ (1985) Vibrational spectra of magnesite ($MgCO_3$) and calcite-III at high pressures. Am Mineral 70:590–600

McCammon C, Hutchison MT, Harris JW (1997) Ferric iron content of mineral inclusions in diamonds from Sao Luiz: a view into the lower mantle. Science 278:434–436

Oelkers EH, Cole DR (2008) Carbon dioxide sequestration a solution to a global problem. Elements 4:305–310

Oganov AR, Ono S, Ma Y, Glass CW, Garcia A (2008) Novel high-pressure structures of $MgCO_3$, $CaCO_3$, and CO_2 and their role in Earth's lower mantle. Earth Planet Sci Lett 273:38–47

Oh KD, Morikawa H, Iwai S, Aoki H (1973a) Hydrothermal growth of magnesite single crystals. Am Mineral 58:339–340

Oh KD, Morikawa H, Iwai S, Aoki H (1973b) The crystal structure of magnesite. Am Mineral 58:1029–1033

Pal'yanov YN, Sokol AG, Borzdov YM, Khokhryaov AF, Sobolev NV (1999) Diamond formation from mantle carbonate fluids. Nature 400:417–418

Perrin J, Vielzeuf D, Laporte D, Ricolleau A, Rossman GR, Floquet N (2016) Raman characterization of synthetic magnesian calcites. Am Mineral 101(11):2525–2538

Poli S, Schmidt MW (2002) Annual review of earth and planetary sciences. Annu Rev Earth Planet Sci 30:207–235

Rividi N, van Zuilen M, Philippot P, Menez B, Godard G, Poidatz E (2010) Calibration of carbonate composition using micro-Raman

analysis: application to planetary surface exploration. Astrobiology 10:293–309

Rohrbach A, Schmidt MW (2011) Redox freezing and melting in the Earth's deep mantle resulting from carbon–iron redox coupling. Nature 472:209–212

Rutt HN, Nicola JH (1974) Raman spectra of carbonates of calcite structure. J Phys C Solid State Phys 7:4522–4528

Schauble EA, Ghosh P, Eiler JM (2006) Preferential formation of C-13–O-18 bonds in carbonate minerals, estimated using first-principles lattice dynamics. Geochim Cosmochim Acta 70(10):2510–2529

Seto Y, Hamane D, Nagai T, Fujino F (2008) Fate of carbonates within oceanic plates subducted to the lower mantle, and a possible mechanism of diamond formation. Phys Chem Minerals 35:223–229

Skorodumova NV, Belonoshko AB, Huang L, Ahuja R, Johansson B (2005) Stability of the $MgCO_3$ structures under lower mantle conditions. Am Mineral 90:1008–1011

Stagno V, Tange Y, Miyajima N, McCammon CA, Irifune T, Frost DJ (2011) The stability of magnesite in the transition zone and the lower mantle as function of oxygen fugacity. Geophys Res Lett 38(19):570–583

Wagner JM (2000) On the inadequacy of linear pressure dependence of vibrational frequency. Solid State Commun 116:355–356

Williams Q, Collerson B, Knittle E (1992) Vibrational spectra of magnesite (MgCor) and calcite-III at high pressures. Am Mineral 77:1158–1165

Zhang J, Martinez I, Guyot F, Gillet P, Saxena SK (1997) X-ray diffraction study of magnesite at high pressure and high temperature. Phys Chem Minerals 24:122–130

Zhang J, Martinez I, Guyot F, Reeder R (1998) Effects of Mg–Fe^{2+} substitution in calcite-structure carbonates: thermoelastic properties. Am Mineral 83:280–287

Zolotoyabko E, Caspi EN, Fieramosca JS, Von Dreele RB, Marin F, Mor G, Addadi L, Weiner S, Politi Y (2010) Differences between bond lengths in biogenic and geological calcite. Cryst Growth Des 10(3):1207–1214